INNOVATION INDUSTRY CONSTRUCTION CONGRESS
SANTANDER / 1 - 5 JUNE 2026
PAÍS INVITADO CHILE

EXPERIMENTAL INVESTIGATIONS OF STRUCTURAL HEALTH MONITORING ON PRESTRESSED CONCRETE RAILWAY SLEEPERS FOR ADVANCED BRIDGE MONITORING APPLICATIONS

Maxime Elias ASMUSSEN[1], Gerd MANTHEI[2], Manuel KOOB[1], Niklas LINGNER[1], Joaquín DÍAZ[1], Jens MINNERT[1]

[1] THM, University of Applied Sciences, Department of Civil Engineering, Giessen, Germany, jens.minnert@bau.thm.de
[2] THM, University of Applied Sciences, Department of Mechanical and Energy Engineering, Giessen, Germany, gerd.manthei@me.thm.de

Abstract

This study experimentally and numerically investigates the bending behavior of prestressed concrete sleepers, focusing on crack formation and associated deformation behavior. The objective is to analyze the structural response under bending stress and to validate the numerical model against experimental results.
An experimental program was developed in accordance with relevant standards to examine the bending crack formation and deformation behavior of prestressed concrete construction elements. Acoustic emission monitoring was employed to observe fracture processes in real time. To detect microcracking during loading broadband AE sensors were used which were especially developed for the detection of microcracks in concrete.
Nonlinear finite element models, based on experiments, were used to study the influence of reinforcement layout and bar diameter on crack initiation. Results show increased bending stiffness and delayed cracking. The intention is to apply these findings to structural health monitoring of concrete bridges and to optimize the analysis using AI-based systems.

Keywords: three-point bending test, digital image correlation, acoustic emission, nonlinear numerical simulation.

1 Introduction

Prestressed concrete sleepers installed on a ballast superstructure constitute the structural basis of railway tracks in Germany as well as in many other countries. Concrete has been an established and approved material for sleeper production for several decades. Nevertheless, damage to sleepers occurs frequently, and the underlying causes are not always fully understood. Throughout their service life, sleepers are subjected to substantial mechanical loads, with train speeds reaching up to 280 km/h and axle loads of 25 t. The German rail network comprises approximately 80 million sleepers, of which around 2% exhibit damage. Roughly 1.4 million of the affected sleepers are prestressed concrete sleepers, most of which display longitudinal cracking along the prestressing steel tendons [1, 2].

Assessing, interpreting, and repairing cracks in prestressed concrete sleepers is a labor-intensive and costly process. The replacement of individual defective sleepers is likewise associated with significant logistical effort. To improve the understanding of crack initiation and growth in prestressed sleepers, acoustic emission (AE) monitoring is employed. AE offers the advantage of detecting crack formation at very early loading stages—well before any visible surface damage occurs, making it a valuable tool not only for research but also for the approval and quality

assurance of prestressed sleepers. Insights gained from AE analysis can help prevent manufacturing defects and support the inspection of components prior to installation.

In total, four three-point bending tests were conducted on prestressed concrete railway sleepers. Three of these tests were deliberately stopped at an applied load of 73 kN to experimentally determine key material parameters, which were subsequently used as input for the simulation model. In the present study, the fourth test was carried out to monitor crack initiation and propagation up to final failure using AE techniques [3, 4].

AE has been successfully applied across a wide range of materials, including steel, concrete, and composites, for the detection and characterization of damage. It enables real-time identification of internal failure processes and is widely used in industrial production for quality control and process optimization. Although AE is also considered promising for assessing the condition of reinforced concrete structures, previous applications have often relied on simplified evaluation methods that do not fully exploit the method's potential. The main challenges arise from the heterogeneous nature of concrete, the attenuation of high-frequency signals, and the geometric complexity of structural components.

2 Experimental setup

2.1 Test setup

The static test for assessing negative bending moments at the center of the sleeper was carried out in compliance with DIN EN 13230-2, the European standard adopted by the German Institute for Standardization for prestressed monoblock concrete sleepers of Type B 70 (track gauge 1,435 mm). This standard specifies the applicable testing procedures and acceptance criteria [5]. The purpose of the test was to induce a defined tensile stress at the upper surface of the sleeper's mid-section. For this purpose, the load was applied in a three-point bending setup with the sleeper positioned upside down. The test setup used in the THM laboratory is illustrated in Figure 1.

Figure 1. Test setup for the three-point bending test in a front view

The tests were carried out using a test portal equipped with a clamping frame. The load was applied by a hydraulic actuator (maximum capacity 520 kN, stroke 250 mm) through a steel profile, adapter plates, and bearings in accordance with [5]. An elastic pad was positioned between the rocker bearing and the sleeper to ensure proper load transfer. The sleeper was supported at the rail seats with a spacing of 1.5 m, and the standard rail seat inclination of 1:40 was compensated using pads and plates [5]. This configuration ensured orthogonal loading and allowed for a maximum test height of 355 mm.

2.2 Digital image correlation measurements

Digital Image Correlation (DIC) is used to record three-dimensional deformations, crack widths, and strain fields. For capturing the specimen surface four 12-MP cameras arranged in a linear configuration are used. This setup minimizes distortions that would otherwise occur if the cameras were positioned at steep angles. At the same time, doubling the number of cameras and reducing the distance to the concrete sleeper improves correlation quality and increases measurement accuracy [6]. To provide adequate contrast for image correlation, the surface is coated with a white base layer and a stochastic speckle pattern, as shown in Figure 2. This enables reliable documentation of visible macro-cracks forming on the specimen surface.

Using image correlation algorithms, it is thus possible to evaluate the recorded images. For this purpose, the evaluation software compares the recorded images of the test body under load with a reference image in an unloaded state.

Figure 2. Stochastic speckle pattern at sleeper's surface

2.3 Acoustic emission measurements

In a previous project [7, 8, 9], broadband AE sensors (up to 200 kHz) were developed specifically for use in concrete. Sixteen of these sensors were installed between the supports in the region of maximum bending moment. For mounting, 2 mm steel plates were bonded to the sleeper surface, and the sensors were coupled using Vaseline. The sensor positions (red) and the four ultrasonic transmitters (blue) are shown in Figure 3. The sensors were arranged in four vertical levels at ± 150 mm and ± 350 mm in the x-direction, with the coordinate origin located at the sleeper center.

The data acquisition system recorded AE signals at 10 MHz sampling rate and 16-bit resolution, using 40 dB preamplification and a 20–200 kHz band-pass filter. Four ultrasonic transmitters (Type V103) mounted on the top surface (blue dots) generated artificial signals to determine wave velocities required for source localization [9].

3 Measurement Procedure, Evaluation, and Validation

3.1 Test Procedure

The static test procedure involving a negative bending moment at the sleeper midspan for type approval is shown in Fig. 4. The test was conducted in accordance with DIN EN 13230-2 [5] to determine the initial negative reference test force at the sleeper midspan, Fc_{0n}. In this diagram,

the applied load (1) is plotted as a function of time (2). The load was increased at a constant rate (3) until the initial negative reference test force Fc_{0n} was reached. This load was then held for a defined period during which the concrete sleeper was inspected for cracks.

Subsequently, the load was increased in increments at the same rate, with holding periods (4) applied at each increment, as shown in Figure 4. During the test, the load at first crack formation Fc_{rn} and the ultimate load Fc_{Bn} were recorded. The acceptance criterion required that the sleeper remain free of cracks up to Fc_{0n}. Fulfilment of this requirement qualifies the corresponding sleeper type for approval.

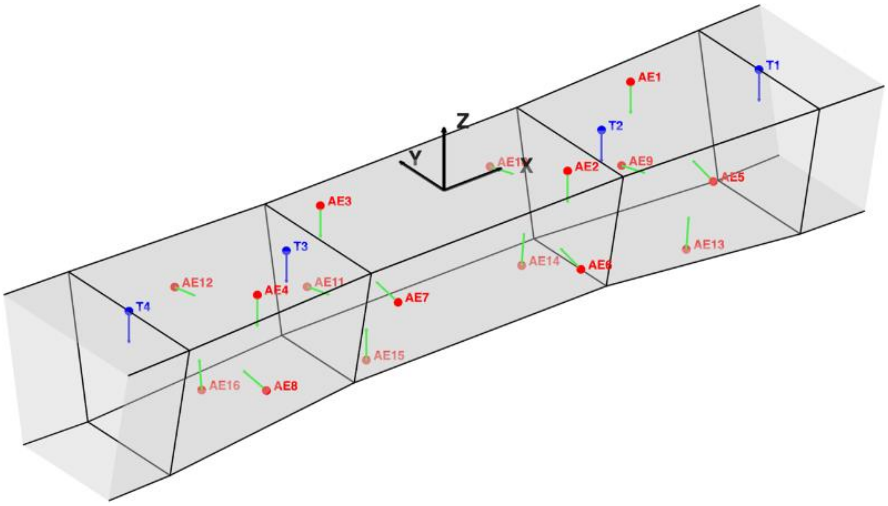

Figure 3. Front and top views of the concrete sleeper showing the positions of the 16 AE sensors (red dots) and the four V103 ultrasonic transmitters (blue dots). The coordinate origin is located at the center of the sleeper's top surface (black cross). Small arrows indicate the normal vectors of the sensors, representing their directions of maximum sensitivity to longitudinal waves [4].

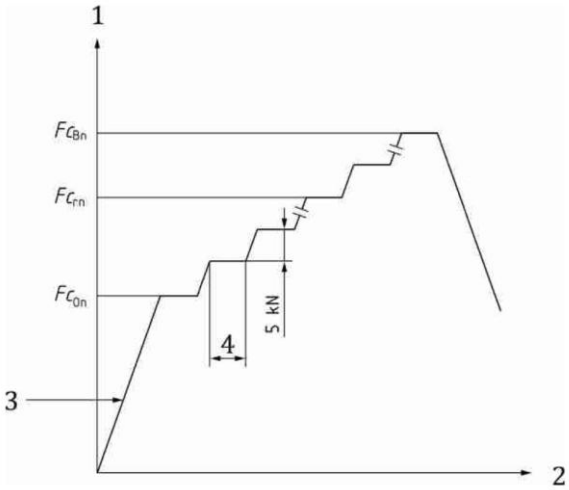

Figure 4. Test procedure in accordance with DIN EN 13230-2 [5]: (1) force, (2) time, (3) maximum loading rate 2 kN/s, (4) load holding time up to 5 min.

3.2 Evaluation of Measurement

3.2.1 Introduction

In accordance with standard [5], the experiment was accompanied by DIC and AE measurements. The total duration of the experiment was approximately 1.7 hours. From a load level of 5 kN onward, the force was increased under force-controlled conditions at a constant rate of 0.05 kN/s. Beginning at the initial negative reference test force Fc_{0n} = 43 kN, the load was applied in increments of 5 kN, with 5-minute holding periods introduced at each increment to perform ultrasonic transmission measurements. Each measurement lasted about 2 minutes. At approximately the ultimate load Fc_{Bn} = 107 kN, failure of the concrete sleeper occurred (see Fig. 5).

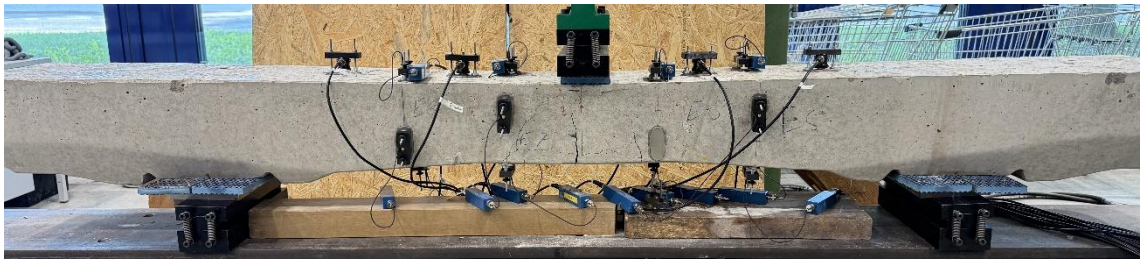

Figure 5. specimen after reaching its ultimate load Fc_{Bn} = 107 kN, showing pronounced cracking and visible structural failure at midspan [3].

3.2.2 Digital image correlation

During the loading phase, the structural response of the concrete sleeper was captured using four 12-MP cameras connected in series. In this work, the Q400 system from Limess Messtechnik & Software GmbH [10] was used in combination with the ISTRA 4D evaluation software [11]. The image acquisition system operated at a frame rate of 0.5 frames per second, providing a continuous record of the deformation behavior throughout the active loading periods. Data collection was temporarily suspended during the load-holding phases to avoid unnecessary storage of redundant images and to ensure that only mechanically relevant deformation states were documented.

Before each experiment, the camera system was calibrated specifically for the respective specimen. This calibration procedure ensured accurate spatial referencing across all four cameras, enabling reliable three-dimensional correlation of the recorded images during subsequent digital image correlation (DIC) analysis.

3.2.3 Acoustic emission analysis

Throughout the experiment, AE activity was monitored using a trigger-based acquisition scheme, while continuous full-waveform recordings were stored for subsequent detailed evaluation. The analysis concentrated on reconstructing the three-dimensional source locations of AE events to map the spatial progression of cracking. For this purpose, an automated localization tool developed by GMuG (Germany) was employed. The procedure requires reliably identified arrival times of both longitudinal (L) and transverse (T) waves. Localization calculations were performed

using experimentally determined wave velocities of 4.85 mm/µs for L-waves and 2.9 mm/µs for T-waves.

A localization result was accepted only if the computed residual error, defined as the mean deviation between measured and theoretical arrival times, remained below a predefined tolerance of a few millimeters to centimeters, and if more than five combined L- and T-wave arrivals contributed to the solution. Events that did not satisfy these conditions were excluded from further analysis. The temporal progression of the cumulative number of located AE events is shown in Figure 6.

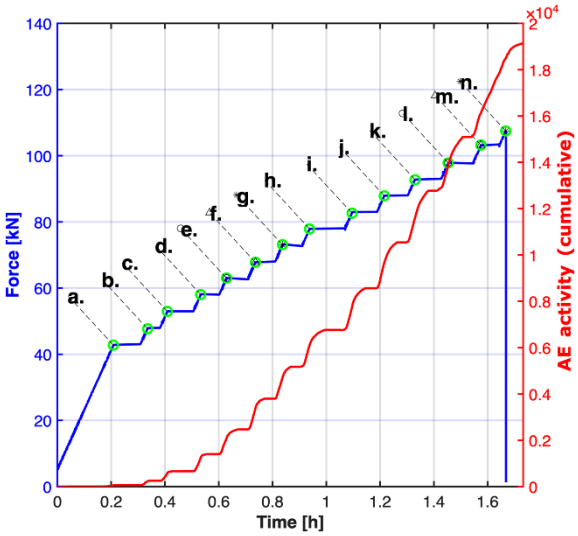

Figure 6. Temporal progression of the cumulative number of located AE events (red curve) and force (blue curve) over time. The load increments of 5 kN are marked by green circles at pos. a. to n. with holding periods of 5 min [4].

3.3 Nonlinear numerical simulation model

A numerical analysis that incorporates realistic material models allows for a detailed assessment of the load-bearing behavior of structural components as well as for the reproduction of experimental results. Such simulations, however, require profound validation. Besides the material properties of the construction materials, boundary conditions, such as the FE mesh size or the stiffness of the supports, have a considerable influence on the numerical outcome. Furthermore, a numerical calculation model is well suited for the preliminary design of experimental test series and for determining relevant test parameters.

In all cases, the numerical model represents an idealized representation of the component. Defects such as gravel pockets or production-related dimensional deviations are not included. In physical component tests, however, such imperfections frequently affect the structural response. These influences are accounted for through parametric studies with modified input parameters. The selected material parameters are summarized in Table 1.

The load-bearing behavior in this study was analyzed using the FE software ATENA developed by Červenka Consulting [12]. Detailed program settings and modeling parameters are provided in [13].

4 Results

4.1 Results of digital image correlation

DIC measurements were carried out on a sleeper from the same production batch and under comparable loading conditions. To prevent any interference from AE sensors, this specimen was tested without AE instrumentation. The loading procedure was terminated at the onset of plastic deformation at 73 kN rather than continued to failure, meaning that DIC data are only available for the initial portion of the loading history.

Figures 8a and 8b present the sleeper on the left, including the DIC-derived deformation field at midspan (blue region), and on the right the corresponding crack widths and deflections recorded at 58 kN and 73 kN. Up to an applied load of 48 kN, the sleeper behaves in a linear-elastic manner. This phase concludes with the formation of the first flexural crack at midspan [9, 10].

As the load increases to 73 kN, three distinct flexural cracks develop (see Fig. 7b, left). The spacing between adjacent cracks ranges from approximately 12 cm to 15 cm, which corresponds to the transfer length required for the reinforcement to reintroduce stress into the surrounding concrete. The maximum measured crack opening and midspan deflection reach about 0.2 mm and 2.2 mm, respectively.

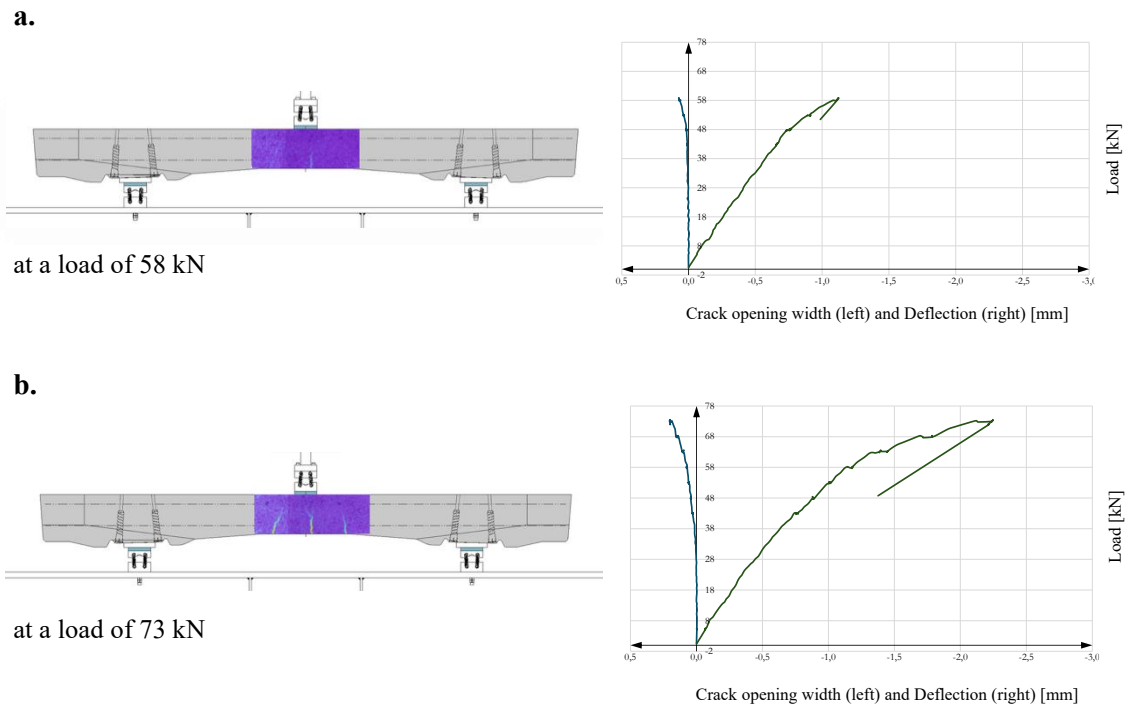

Figure 7. Railway sleeper with the results of the DIC measurements at the center (blue area) and measured crack opening width and deflection (right-hand side) at load of 58 kN (a.) and 73 kN (b.) [3].

4.2 Results of AE measurements

The right ordinate in Fig. 4 (red) shows how the cumulative number of located AE events evolves over time during the static three-point bending test. In total, more than 33,000 AE signals were detected, indicating pronounced microstructural activity within the sleeper. Of these, over 19,000 events could be localized with sufficient accuracy, each based on at least six L- and T-wave arrivals, allowing a detailed spatial reconstruction of crack development. The curves illustrate that AE activity begins once the load reaches Fc_{0n} = 43 kN and increases disproportionately with further loading. A stepped progression is observed: AE activity pauses during the load-holding phases and resumes with each new load increment. Shortly before ultimate failure, the number of events rises sharply, reflecting accelerated crack growth and the imminent collapse of the specimen.

Figure 8 presents the 19,135 reliably located AE events (black dots), each determined from at least six wave onsets, projected onto the three principal coordinate planes (top view and two side views). The outline of the sleeper is shown by black lines, and the sensor positions are indicated by red dots. The spatial distribution of events is clearly non-uniform. Instead, distinct clusters emerge, particularly evident in the top-view projection in the upper left of Fig. 6, where five concentrated regions of AE activity can be identified. These clusters correspond to localized zones of elevated stress caused by the applied bending moment, where microcracking initiates and progressively intensifies. The accumulation of events within these regions marks the transition from diffuse microcracking to more localized damage, which ultimately governs the crack propagation pattern and the failure mechanism of the sleeper.

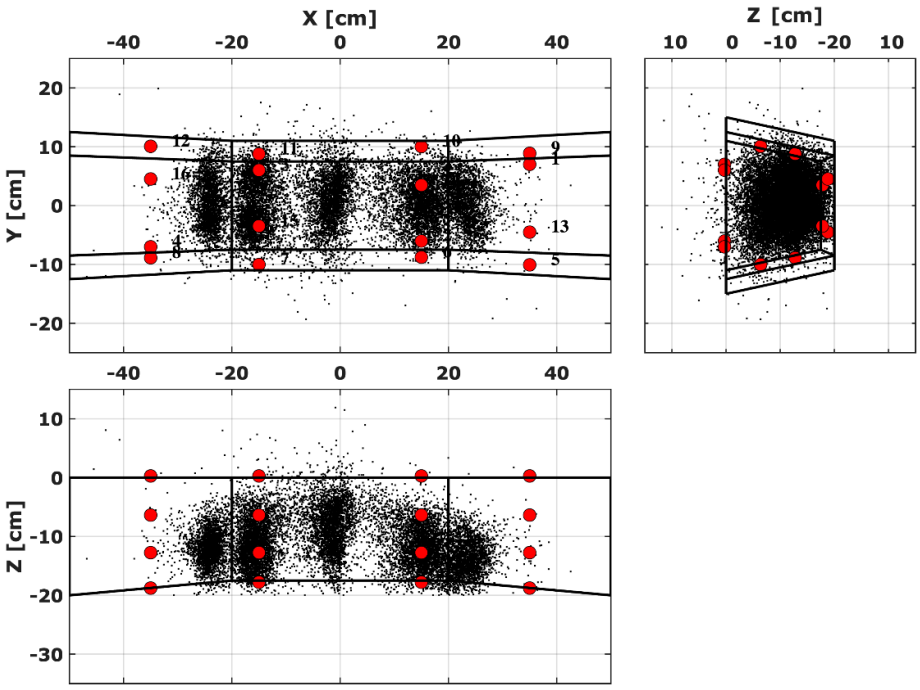

Figure 8. Projection of the localized AE events (black small dots) from the three-point bending test on the railroad sleeper in the top view (x-y plane) and two side views (x-z plane and y-z plane). The contour of the specimen is represented by black lines, and the positions of the AE sensors by red points [4].

4.3 Results of nonlinear numerical calculations

To achieve a better correlation between the experimental and numerical results, the material parameters of the sleeper concrete were determined [3]. These are shown in column 3 of Table 1. Based on these results, a parameter study was carried out with the numerical nonlinear finite elements program ATENA. The objective was to reproduce the experimentally obtained load–deflection curve as accurately as possible.

The vertical deformation shown in Figure 9 was determined using DIC measurement. Figure 9 illustrates that the load–deflection response is captured accurately up to a deflection of approximately 3.5 mm. Beyond this point, the numerical model begins to slightly overestimate the stiffness, continuing to do so until the ultimate load Fc_{Bn} = 107 kN is reached with a deflection of 22 mm. To achieve this result, the material parameters listed in the fourth column of Table 1 were used.

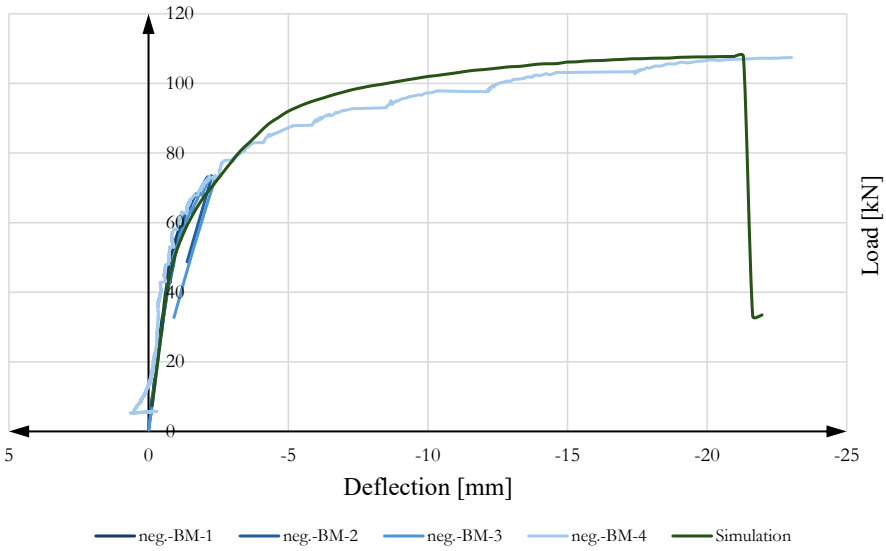

Figure 9. Comparison of measured and simulated load–deflection curves for sleeper tests neg.-BM-1 to neg.-BM-4 under negative bending moment at midspan [3].

Table 1. Parameters of the tested concrete [3]

examination	abbreviation	result	numerical calculation
compressive strength cylinder	$f_{c,m,cyl}$	99.5 MPa	99.5 MPa
elastic modulus	$E_{c,m}$	59.4 GPa	0.8 x 59.4 GPa
prestress	σ_p	0.81 GPa	0.81 GPa
tensile strength	$f_{c,t,m}$	7.67 MPa	0.7 x 7.67 MPa

To enable a meaningful comparison between the measured and simulated crack-opening widths, the FEM results obtained with ATENA are presented as color maps in Figure 10. In the FEM analysis, the first crack forms at a load of 43.8 kN (Fig. 10a.) with an initial crack-opening width of 0.04 mm. At 73.6 kN, five flexural cracks have developed, exhibiting a maximum width of approximately 0.45 mm and a spacing of about 10 cm (Fig. 10b.). At ultimate failure, the simulation predicts multiple flexural cracks, with the central cracks merging into a diagonally oriented crack network in the upper region of the cross-section (Fig. 10c.). The maximum simulated crack-opening width reaches 6.97 mm at a midspan deflection of 21.95 mm. Experimentally, failure occurs at approximately 107 kN with a deflection of 23.02 mm, accompanied by a comparable crack pattern as identified through AE analysis (Fig. 8) and visually (Fig. 5).

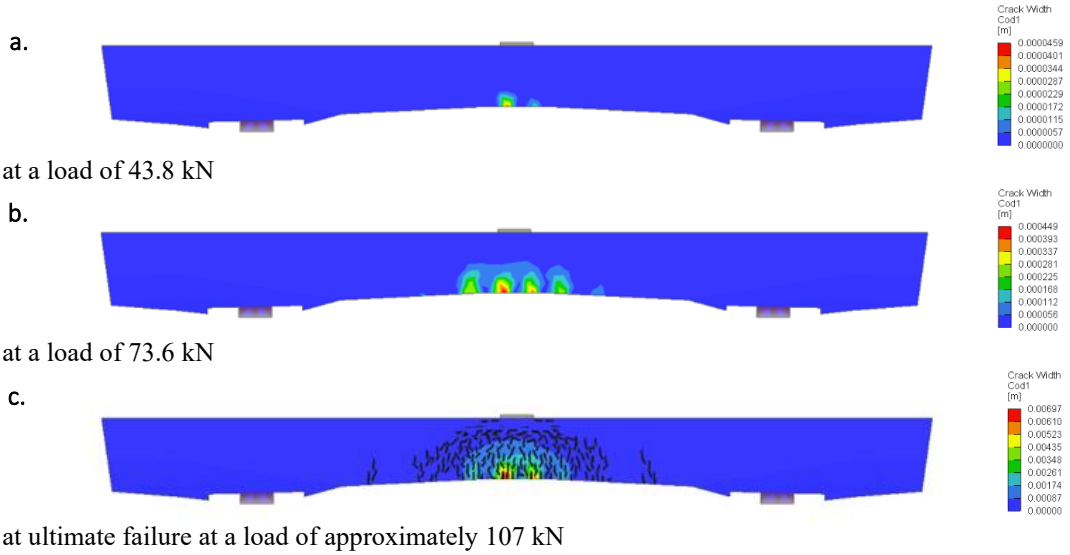

Figure 10. Calculated crack opening width as color maps at loads of 43.8 kN (a.), 73.6 kN (b.), and 107 kN (c.) [3].

In a parametric study, the validated numerical model was employed to examine the influence of the reinforcement bar diameter and its arrangement on crack initiation. The analysis revealed that variations in the bar diameter had no notable effect on the initiation of cracking. In contrast, adjustments to the reinforcement layout resulted in increased flexural stiffness and a delayed initiation of cracking, indicating a measurable impact of the reinforcement configuration on the structural response.

5 Conclusions

The experimental investigations provide a detailed understanding of the structural behavior of prestressed concrete railway sleepers subjected to static bending. By combining digital image correlation (DIC), acoustic emission (AE) monitoring, and nonlinear finite element (FEM) analysis, the study offers a comprehensive assessment of crack initiation, propagation, and failure mechanisms.

AE monitoring demonstrated a high sensitivity to early-stage damage, capturing microcrack formation well before surface cracks became visible and prior to the first crack openings detected by DIC. The three-dimensional localization of AE events enabled precise spatial mapping of crack

initiation zones and subsequent crack growth along the tensile region of the sleeper. Complementary DIC measurements confirmed the development of flexural cracks and provided quantitative information on crack widths and midspan deflections.

The nonlinear FEM model developed in ATENA reproduced the global load–deflection response, crack evolution, and failure pattern with good overall agreement. While slight deviations in stiffness and crack-opening magnitudes were observed, primarily attributable to uncertainties in material parameters, boundary conditions, and experimental scatter, the numerical model successfully captured the essential structural behavior. Iterative calibration of material properties and support conditions proved essential for achieving close correspondence between simulated and experimentally measured load–deflection curves, underscoring the importance of validated input data for reliable numerical modeling.

Most AE events were localized between the supports and the load introduction points, forming cloud-like clusters due to inherent localization uncertainties. Nevertheless, the spatial distribution of AE activity corresponded well with the crack patterns observed experimentally and predicted numerically. The combined evaluation of AE, DIC, and FEM results highlights the potential of AE monitoring as a powerful tool for early detection of microcracking in prestressed concrete sleepers. While current quality-control procedures focus primarily on the absence of visible cracks up to the first reference load, AE monitoring provides deeper insight into internal damage processes and may, in the long term, support or even replace existing assessment criteria.

The present study is limited to static bending tests under controlled laboratory conditions. In service, railway sleepers are subjected to dynamic loading, environmental influences, and long-term degradation mechanisms such as creep and fatigue, all of which may significantly affect crack formation and durability. To develop robust predictive models and practical structural health monitoring (SHM) strategies, further research is required, including larger sample sizes, dynamic and cyclic loading scenarios, and long-term exposure studies. The findings presented here should therefore be regarded as conditionally valid but provide a solid foundation for future investigations aimed at improving the assessment, monitoring, and long-term performance evaluation of prestressed concrete railway sleepers.

6 Outlook

The findings obtained from prestressed concrete railway sleepers provide a solid basis for transferring advanced monitoring concepts to existing bridge structures. The demonstrated sensitivity of acoustic emission monitoring to early microcracking, together with deformation measurements from digital image correlation and validated nonlinear finite element modeling, establishes a coherent framework for structural assessment. Future research should apply this framework to prestressed concrete bridges in service, where dynamic loads, environmental influences, and long-term degradation govern damage evolution. Integrating these techniques with AI supported data interpretation and digital twin models will be essential for continuous condition assessment and more reliable predictions of remaining service life. This approach offers a promising pathway toward next generation structural health monitoring of aging bridge infrastructure.

Acknowledgement

The authors gratefully acknowledge the financial support provided by the Research Campus of Central Hessen within the framework of the funding program Experimentation Spaces (Project No. 2025_1_03). We also sincerely thank Scheld Construction Company GmbH, Biedenkopf, Germany, for supplying the railway sleepers and delivering them to the laboratory of the Department of Civil Engineering of THM.

References

[1] Hentschel, V. (2017). Fahrwegstrategie der DB Netz AG – Anlagenverfügbarkeit im Lebenszyklus: Impulsreferat – 3. Symposium Lebenszyklus System Betonschwelle 2017 [Conference presentation].
[2] Haban, F. X. (2016). Theoretische und experimentelle Untersuchungen an Spannbetonschwellen (Doctoral dissertation, Technische Universität München). https://nbn-resolving.org/urn:nbn:de:bvb:91-diss-20160927-1303754-1-8
[3] Asmussen, M. E. (2025). Experimental and numerical investigations of the static bending crack and deformation behavior of prestressed concrete railway sleepers (master's thesis, Technische Hochschule Mittelhessen, Institute for Structural Engineering).
[4] Manthei, G., Asmussen, M. E., Koob, M., Hoss, L., Minnert, J., & Lademann, F. (2026). Structural Health Monitoring of Prestressed Concrete Railway Sleepers using Acoustic Emission Testing during Static Bending Test. Submitted to *12th European Workshop on Structural Health Monitoring, 7-10 July 2026, Toulouse, France*
[5] Deutsches Institut für Normung e. V. (2016). DIN EN 13230-2:2016-11. Railway applications – Track – Concrete sleepers and bearers – Part 2: Prestressed monoblock sleepers (German version EN 13230-2:2016).
[6] Lichtenberger, R., & Siebert, T. (2015). 3D Verformungsmessung mit mehr als 2 Kameras und digitaler Bildkorrelation. Modellansatz und Anwendung. *Fachseminar Optische Prüf- und Messverfahren, 17, 18.*
[7] Manthei, G., Koob, M., Walther, M., Minnert, J., & Moriya, H. (2018). Acoustic emission measurements during three-point bending fatigue test on a prestressed reinforced concrete railroad sleeper. In *Progress in Acoustic Emission XIX, Proceedings of the International Acoustic Emission Conference, Sapporo, Japan* (pp. 1-9).
[8] Manthei, G., Koob, M., Bohn, D., Lingner, N., & Minnert, J. (2024). Acoustic Emission Measurements During a Four-Point Bending Test on a Reinforced Concrete Specimen. 36th Conference of the European Working Group on Acoustic Emission, 18-20 September 2024, Potsdam, Germany. *e-Journal of Nondestructive Testing* Vol. 29(10). https://doi.org/10.58286/30271
[9] Manthei, G., Koob, M., Lingner, N., & Minnert, J. (2025). Acoustic Emission and Ultrasonic Transmission Measurements in a Large-Scale Reinforced Concrete Specimen. In *Progress in Acoustic Emission XXI (S. 25–31).*
[10] Lichtenberger, R. (2018). Limess – Kompetenz in kamerabasierten Messsystemen. https://www.limess.com/de/component/jdownloads/send/12-q400/5-q400-flyer-deutsch
[11] Dantec Dynamics GmbH (2016). ISTRA 4D Software Manual Q-4XX Sytem
[12] Červenka, V., Jendele, L., & Červenka, J. (2025). ATENA Program Documentation Part 1: Theory
[13] Červenka, J., & Jendele, L. (2025). ATENA Program Documentation Part 6: ATENA Input File Format